

Experimental Investigation on the Fatigue Mechanical Properties of Intermittently Jointed Rock Models Under Cyclic Uniaxial Compression with Different Loading Parameters

Yi Liu¹ · Feng Dai¹ · Lu Dong² · Nuwen Xu¹ · Peng Feng¹

Received: 9 March 2017 / Accepted: 12 September 2017 / Published online: 20 September 2017
© Springer-Verlag GmbH Austria 2017

Abstract Intermittently jointed rocks, widely existing in many mining and civil engineering structures, are quite susceptible to cyclic loading. Understanding the fatigue mechanism of jointed rocks is vital to the rational design and the long-term stability analysis of rock structures. In this study, the fatigue mechanical properties of synthetic jointed rock models under different cyclic conditions are systematically investigated in the laboratory, including four loading frequencies, four maximum stresses, and four amplitudes. Our experimental results reveal the influence of the three cyclic loading parameters on the mechanical properties of jointed rock models, regarding the fatigue deformation characteristics, the fatigue energy and damage evolution, and the fatigue failure and progressive failure behavior. Under lower loading frequency or higher maximum stress and amplitude, the jointed specimen is characterized by higher fatigue deformation moduli and higher dissipated hysteresis energy, resulting in higher cumulative damage and lower fatigue life. However, the fatigue failure modes of jointed specimens are independent of cyclic loading parameters; all tested jointed specimens exhibit a prominent tensile splitting failure mode. Three different crack coalescence patterns are classified between two adjacent joints. Furthermore, different from the progressive failure under static monotonic loading, the jointed rock specimens under cyclic compression fail more abruptly without evident preceding signs.

The tensile cracks on the front surface of jointed specimens always initiate from the joint tips and then propagate at a certain angle with the joints toward the direction of maximum compression.

Keywords Fatigue mechanical properties · Intermittently jointed rocks · Cyclic loading parameters · Uniaxial compression

1 Introduction

The mechanical characteristics of intermittently jointed rocks play a dominant role in the overall mechanical behavior of many mining and civil engineering structures, such as underground tunnels, bridge abutments, and road foundations. Since these rock structures are likely to be subjected to cyclic loading resulting from earthquakes, quarrying, and rockbursts, it is thus crucial to accurately characterize the fatigue properties and failure mechanism of intermittently jointed rocks for the rational design and long-term stability analysis of rock structures under different cyclic loading conditions.

Existing attempts to understand the mechanical properties of jointed rocks were mainly concentrated on static loading. Researchers have performed numerous physical experiments on rock models containing various joints, including static uniaxial compression tests (Kulatilake et al. 1997, 2001; Singh et al. 2002; Bahaaddini et al. 2013; Fan et al. 2015; Feng et al. 2017), biaxial or triaxial compression tests (Einstein and Hirschfeld 1973; Tiwari and Rao 2006; Prudencio and Van Sint 2007; Sagong et al. 2011), and direct shear tests (Lajtai 1969; Gehle and Kutter 2003; Zhang et al. 2006; Park and Song 2009; Bahaaddinia et al. 2014). They concluded that the static strength and the deformation

✉ Feng Dai
fengdai@scu.edu.cn

¹ State Key Laboratory of Hydraulics and Mountain River Engineering, College of Water Resource and Hydropower, Sichuan University, Chengdu 610065, Sichuan, China

² PLA University of Science and Technology, Nanjing 210007, Jiangsu, China

behavior of jointed rocks were significantly affected by the geometrical parameters of the joints, involving joint length, orientation, spacing and density, etc. In addition, the fracture coalescence behavior of jointed rock specimens was systematically assessed under uniaxial or biaxial compression (Bobet and Einstein 1998; Wong and Chau 1998; Wong et al. 2001; Sagong and Bobet 2002; Wong and Einstein 2009a, b, c); they first identified the nature of the coalescence cracks and proposed associated coalescence classification schemes. Wong and Einstein (2009a, b, c) further improved the classification scheme to describe the newly identified crack types and features. Recently, combining the numerical approaches, the progressive failure process of rocks containing single, two, or multiple joints were revealed under static loading conditions (Wong et al. 2006; Zhang and Wong 2012, 2013; Bi et al. 2016; Cao et al. 2016).

Compared with efforts on studying static mechanical properties of rock materials, investigations of cyclic mechanism were mostly limited to intact rocks. Some early experimental studies revealed the hysteresis of the

stress–strain curve of intact rocks under cyclic loading and reported that the plastic deformation gradually accumulates with increasing number of cycles (Burdine 1963; Attewell and Farmer 1973; Tao and Mo 1990; Ray et al. 1999). Subsequently, Bagde and Petroš (2005a) defined the term “fatigue” as the tendency of materials to fail or the process of damage accumulation under cyclic loading conditions. Researchers further reported that both the fatigue strength and the deformation modulus of intact rocks exponentially decreased with increasing cycles, and the fatigue mechanical properties were significantly affected by cyclic loading parameters, including cyclic frequency, maximum stress and amplitude (Bagde and Petroš 2005b; Fuenkajorn and Phueakphum 2010; Ma et al. 2013; Liu et al. 2017a). To describe the damage evolution of rock materials under cyclic loading, Xiao et al. (2009, 2010) derived an inverted-S fatigue damage model for intact rocks (Fig. 1a). They pointed out that the fatigue damage variable shows a three-phase development with increasing relative cycle (i.e., ratio of the current cycle number

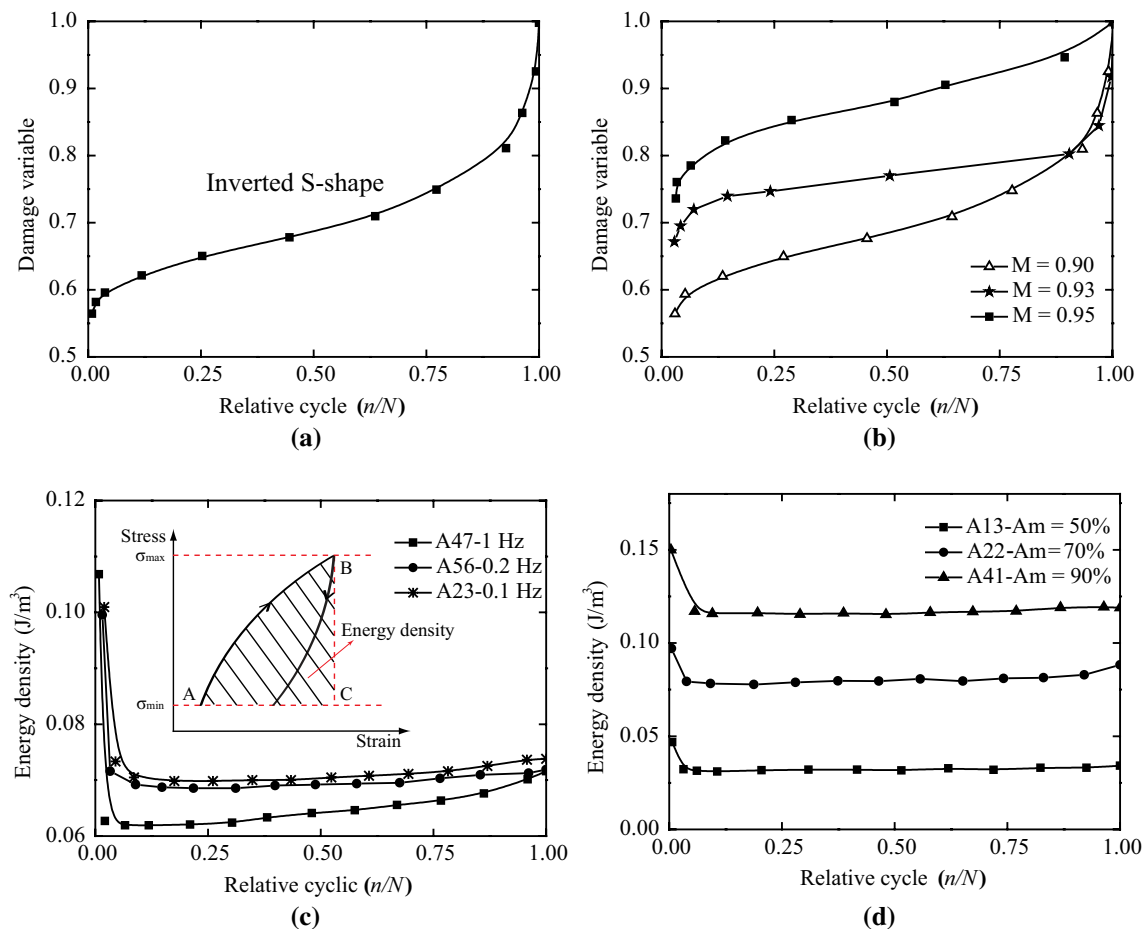


Fig. 1 Schematic of the fatigue damage variable and energy density of the intact rocks under cyclic loading reproduced from previous studies: **a** Xiao et al. (2009); **b** Xiao et al. (2010); **c** and **d** Momeni et al. (2015)

n to the total cycle number N), and it increased with the increase in maximum cyclic stress (Fig. 1b). In addition, the energy characteristics of intact rocks under cyclic loading were investigated (Hua and You 2001; Bagde and Petroš 2009); they reported that the sustained energy of intact rocks could be regarded as a rock characteristic, which affected the rock failure mechanism. Momeni et al. (2015) further reported that a dramatic decrease in the energy density (i.e., areas under the loading portion of the stress–strain curve ranging between minimum and maximum stress, the region ABC in Fig. 1c) occurred for the initial cycles, and the energy density increased with increasing amplitude or decreasing frequency (Fig. 1c, d).

Since the mechanical behavior of jointed rocks significantly differs from that of intact rocks, the fatigue properties of jointed rocks under cyclic uniaxial compression was also investigated (Brown and Hudson 1974; Prost 1988; Li et al. 2001; Liu et al. 2017b). Earlier research (Brown and Hudson 1974; Prost 1988) pointed out that the intermittently jointed rocks were extremely sensitive to cyclic loading and that the fatigue life of jointed rocks increased with decreasing maximum cyclic stress and amplitude. Recently, Li et al. (2001) reported that the cyclic loading frequency significantly affected the fatigue strength and residual strength of jointed rock specimens. Liu et al. (2017b) systematically revealed the influence of joint geometry configurations on the mechanical properties of intermittently jointed rocks under given cyclic loads.

However, according to the available literature, the fatigue responses of intermittently jointed rocks to cyclic loading, including the fatigue deformation characteristic, the fatigue energy and damage evolution, and the fatigue failure and progressive behavior, remain far from being thoroughly understood. The influence of cyclic loading parameters, namely different cyclic frequencies, maximum stresses, and amplitudes, on these fatigue properties have never been systematically investigated in the laboratory. It is thus the intention of this study to experimentally investigate the fatigue mechanical properties of intermittently jointed rock models under cyclic uniaxial compression with different loading parameters.

The remainder of this text is organized as follows. Section 2 introduces the experimental setup, including the specimen preparation, the test equipment, and the test schemes, followed by the determination of fatigue mechanical properties and experimental results of monotonic loading tests in Sect. 3. Section 4 comprehensively analyzes and discusses the experimental results of cyclic uniaxial compression tests, regarding the influence of the three cyclic loading parameters on the fatigue deformation characteristic, the fatigue energy and damage evolution, and the fatigue failure and progressive behavior. Section 5 summarizes the study.

2 Experimental Setup

2.1 Specimen Preparation and Test Equipment

Considering that directly fabricating joints in real rocks is difficult, artificial rock-like materials are thus widely used to prepare jointed rock models in the laboratory investigations ever since the late 1960s (Einstein et al. 1969; Einstein and Hirschfeld 1973; Shen et al. 1995; Bobet and Einstein 1998; Singha and Rao 2005; Wong and Einstein 2009a, b, c). In this study, the synthetic rock-like materials are prepared with fine sand, high-strength cement, water, silicon powder, and water-reducing agent at mass ratio of 1.2:1:0.35:0.15:0.015, respectively, as shown in Fig. 2. The preparation process of the intermittently jointed rock models is as follows: (i) assembling the specified jointed mold (length \times thickness \times height = 200 mm \times 100 mm \times 100 mm) and inserting the steel sheets (length \times thickness \times height = 15 mm \times 0.4 mm \times 150 mm) into corresponding slots pre-fabricated in jointed mold (Fig. 2); (ii) pouring the mixed synthetic materials into the assembled mold, and vibrating the mold with mixed materials for 2 min on a shaking table to minimize air bubbles inside the specimens; (iii) removing these steel sheets after 10 h of curing and disassembling the jointed mold after 24 h of curing; (iv) keeping the cast intermittently jointed rock models for 28 days in a curing room (at 20 °C, 95% relative humidity and an atmospheric pressure). To keep the mechanical properties of the jointed specimens as consistent as possible, the mix proportion of synthetic materials remains the same, and the preparation processes are carefully controlled.

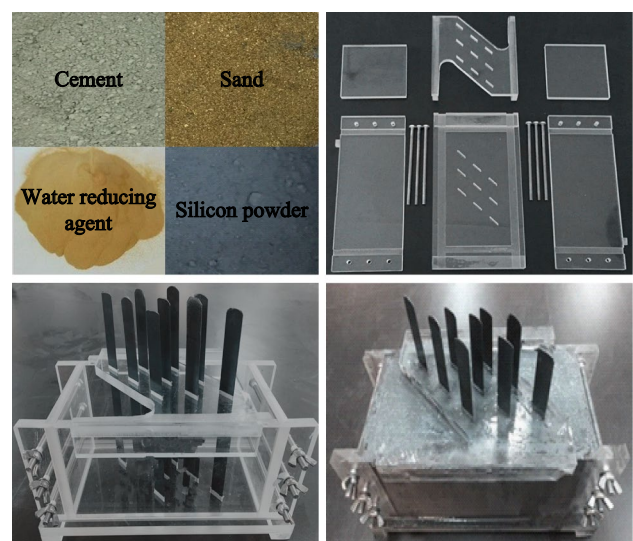


Fig. 2 Sketch of the components of synthetic materials and the mold for fabricating jointed rock models

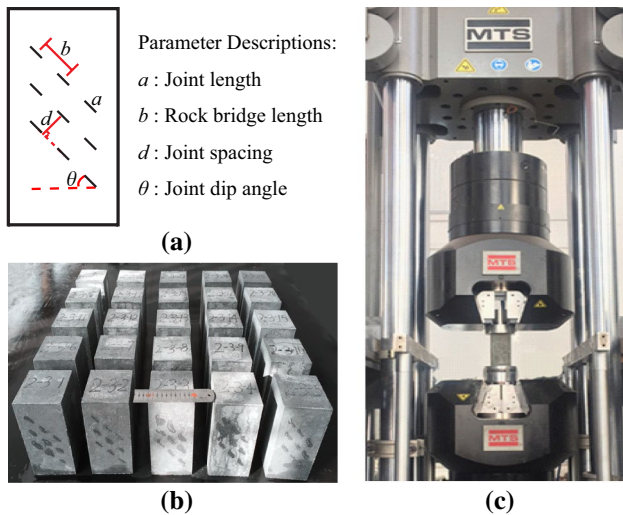


Fig. 3 **a** Schematic of the joint geometrical parameters, **b** the prepared intermittently jointed rock models, and **c** the MTS-793 Rock and Concrete Test System

Figure 3a presents the joint geometry configuration selected in this study, which is determined by the number and position of steel sheets inserted in the jointed molds. All jointed rock models have the same geometry configuration in our tests, including the joint length $a = 15$ mm, the rock bridge length $b = 20$ mm, the spacing $d = 24$ mm, the dip angle $\theta = 45^\circ$, the persistence $k = 0.318$, and the intensity $\rho = 6.75 \times 10^{-3} \text{ mm}^{-1}$. Note that the persistence is defined as the ratio of the sum of individual joint surface areas to the surface of a coplanar reference plane, and the intensity is defined as the total joint area per unit volume (Dershowitz and Einstein 1988). Typical prepared intermittently jointed rock specimens depicted in Fig. 3b, c show the MTS-793 Rock and Concrete Test System employed in our tests. This test system is composed of software and hardware components, which provides a closed-loop control of servo-hydraulic equipment. Consisting of a compression loading frame, an axial dynamic loading system, and a data acquisition system, this equipment is capable of performing uniaxial static and dynamic compression tests. The loading frame has a 2500 KN and a 2750 KN compression load capacity for static and dynamic tests, respectively. The loading mode can be automatically varied via the dynamic control transducers, and the axial deformation and load can be simultaneously recorded by the data acquisition system. Specifically, for cyclic tests, the loading waveform can be selected from ramp, square, and sinusoidal waves, and the loading frequency can be varied from 0.01 to 20 Hz. In addition, in our tests, high vacuum grease is utilized to lubricate the contact surfaces between the tested specimens and the loading plates, and a JAI SP-5000 M high-resolution industrial camera is used to monitor the

cracking process of jointed specimens with images taken at a frame rate of 134 fps.

2.2 Test Procedure and Schemes

To measure the static mechanical properties of the jointed rock models, monotonic uniaxial compression tests are first conducted on four jointed specimens in an axial displacement control mode with a strain rate of $5 \times 10^{-5} \text{ s}^{-1}$. The obtained static uniaxial compression strength provides the reference values of cyclic loading parameters. For the cyclic compression tests, a periodic sinusoidal waveform is specified, and the loading path is shown in Fig. 4, in which the following cyclic loading parameters are defined: T is the cycle period, the frequency F is defined as $F = 1/T$, σ_{\max} and σ_{\min} are the maximum and minimum cyclic stress, respectively, and $\sigma_{\text{amp}} = \sigma_{\max} - \sigma_{\min}$ and $\sigma_{\text{avr}} = (\sigma_{\max} + \sigma_{\min})/2$ denote the cyclic amplitude and the average stress, respectively. Initially, the jointed specimens are loaded from 0 to σ_{avr} at the strain rate of $5 \times 10^{-5} \text{ s}^{-1}$, and then the cyclic loading and unloading are conducted with specified loading parameters.

In this study, 30 cyclic uniaxial compression tests with different loading parameters are performed to investigate the influence of cyclic loading parameters, including different frequencies F of 1, 3, 5, and 10 Hz, different maximum stress levels M of 0.80, 0.85, 0.90, and 0.95 and different amplitude levels A of 0.40, 0.50, 0.60, and 0.70; thereinto, the maximum stress level M and amplitude level A are defined as the ratio of the maximum cyclic stress and amplitude to the static uniaxial compressive strength of jointed rock specimens, respectively. The different cyclic loading conditions are summarized in Table 1, in which specimens M85, A5, and F1 are subjected to the same cyclic loading. For each cyclic loading condition, three jointed specimens are tested.

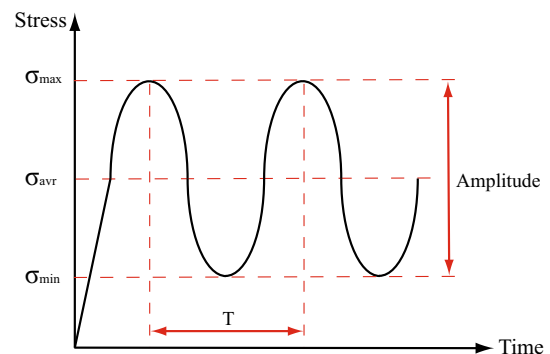


Fig. 4 Schematic of the loading path in cyclic uniaxial compression tests and the characteristic parameters of cyclic loading

Table 1 Summary of the cyclic loading parameters and the representative cyclic testing results

Jointed specimen no.	Cyclic loading parameters	Fatigue failure strain (%)	Post-failure monotonic strain (%)	Deviation (%)	Fatigue life
F1 or M85 or A5	$F = 1 \text{ Hz}, M = 0.85, A = 0.50$	0.53	0.52	1.92	344
F3	$F = 3 \text{ Hz}, M = 0.85, A = 0.50$	0.55	0.52	5.77	561
F5	$F = 5 \text{ Hz}, M = 0.85, A = 0.50$	0.57	0.52	9.62	1036
F10	$F = 10 \text{ Hz}, M = 0.85, A = 0.50$	0.55	0.52	5.77	2532
M80	$M = 0.80, F = 1 \text{ Hz}, A = 0.50$	0.57	0.53	7.55	867
M90	$M = 0.90, F = 1 \text{ Hz}, A = 0.50$	0.50	0.51	-1.96	102
M95	$M = 0.95, F = 1 \text{ Hz}, A = 0.50$	0.53	0.51	3.92	13
A4	$A = 0.40, F = 1 \text{ Hz}, M = 0.85$	0.51	0.52	-1.92	633
A6	$A = 0.60, F = 1 \text{ Hz}, M = 0.85$	0.49	0.52	-5.77	168
A7	$A = 0.70, F = 1 \text{ Hz}, M = 0.85$	0.48	0.52	-7.69	69

3 Determination of Fatigue Properties and Results of Monotonic Loading Tests

3.1 Determination of Fatigue Energy Density and Damage Variable

Based on the first law of thermodynamics, the variation in work of the external forces δW is equal to the variation of internal energy δU for each volume element under adiabatic conditions (static equilibrium and no net heat flow). According to Solecki and Conant (2003), δW can be calculated in terms of the stress components σ and corresponding strain components ϵ as follows:

$$\delta W = \int_V (\sigma_{xx}\delta\epsilon_{xx} + \sigma_{yy}\delta\epsilon_{yy} + \sigma_{zz}\delta\epsilon_{zz} + 2\sigma_{xy}\delta\epsilon_{xy} + 2\sigma_{yz}\delta\epsilon_{yz} + 2\sigma_{zx}\delta\epsilon_{zx})dV \tag{1}$$

Expressing the internal energy U for volume V in terms of the internal energy per unit volume, i.e., the energy density u , there is,

$$\begin{aligned} \delta U &= \int_V \delta u dV \\ &= \int_V (\sigma_{xx}\delta\epsilon_{xx} + \sigma_{yy}\delta\epsilon_{yy} + \sigma_{zz}\delta\epsilon_{zz} + 2\sigma_{xy}\delta\epsilon_{xy} + 2\sigma_{yz}\delta\epsilon_{yz} + 2\sigma_{zx}\delta\epsilon_{zx})dV \end{aligned} \tag{2}$$

Thus, the variation of energy density u can be expressed as follows:

$$\delta u = (\sigma_{xx}\delta\epsilon_{xx} + \sigma_{yy}\delta\epsilon_{yy} + \sigma_{zz}\delta\epsilon_{zz} + 2\sigma_{xy}\delta\epsilon_{xy} + 2\sigma_{yz}\delta\epsilon_{yz} + 2\sigma_{zx}\delta\epsilon_{zx}) \tag{3}$$

For uniaxial compression tests, there is only an axial stress component and a corresponding strain component, and thus the energy density u can be calculated as follows:

$$u = \int_{\epsilon} \sigma d\epsilon \tag{4}$$

For cyclic uniaxial compression tests, the fatigue energy density can be calculated by integrating the fatigue stress–strain curve. As shown in Fig. 5a, the area under the loading curve represents the total energy density u (i.e., the region ABCD), the area under the unloading portion indicates the elastic energy density u^e (i.e., the region CDEF), and the area difference between u and u^e represents the hysteresis energy density u^d (i.e., the region ABCFE); the elastic energy is released in the unloading process, and the hysteresis energy is released inducing the internal damage

and irreversible deformation. The following equations are generally employed to determine the fatigue energy density parameters (Meng et al. 2016):

$$\begin{cases} u = \int_{\epsilon_1}^{\epsilon_m} \sigma d\epsilon = \sum_{i=1}^n \frac{1}{2}(\sigma_{i2} + \sigma_{i1})(\epsilon_{i2} - \epsilon_{i1}) \\ u^e = \int_{\epsilon_2}^{\epsilon_m} \sigma d\epsilon = \sum_{i=1}^n \frac{1}{2}(\sigma_{i2} + \sigma_{i1})(\epsilon_{i2}^e - \epsilon_{i1}^e) \\ u^d = u - u^e = \int_{\epsilon_1}^{\epsilon_m} \sigma d\epsilon - \int_{\epsilon_2}^{\epsilon_m} \sigma d\epsilon \end{cases} \tag{5}$$

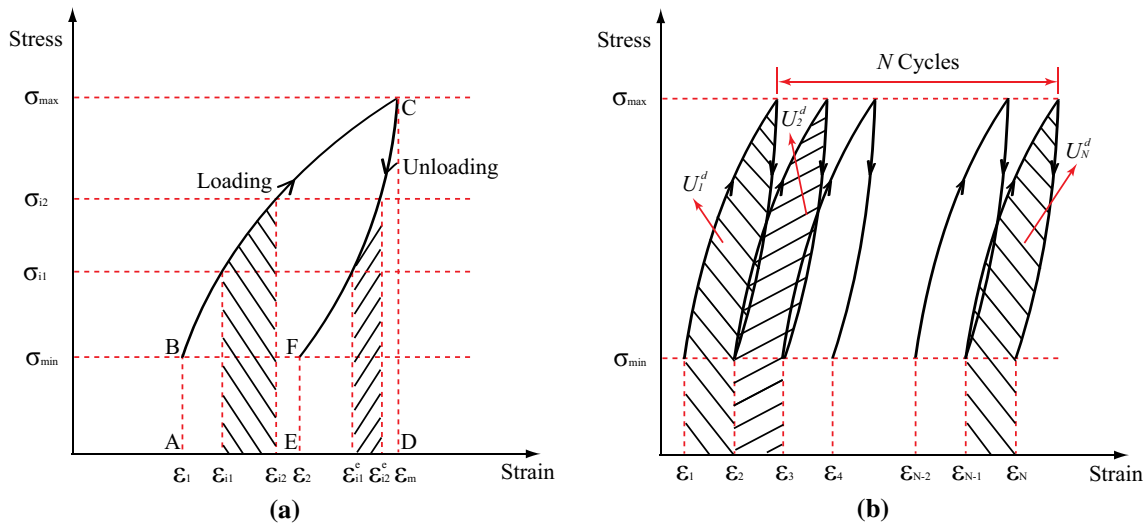


Fig. 5 **a** Calculation of the fatigue energy density parameters, and **b** schematic of determination of the fatigue damage variable

where ϵ_1 and ϵ_2 are the strain corresponding to the minimum stress σ_{\min} in the loading and unloading curve, respectively; ϵ_m is the strain corresponding to the maximum stress σ_{\max} in the loading curve; ϵ_{i1} , ϵ_{i2} , ϵ_{i1}^e , and ϵ_{i2}^e are the strain at an integral step; σ_{i1} and σ_{i2} are the cyclic stress at an integral step, respectively.

The fatigue damage variable, which reflects the accumulated damage evolution of rock materials under cyclic loads, is one of the most critical parameters in fatigue analysis. Xiao et al. (2010) pointed out that the damage variable can be defined based on the hysteresis energy. In this study, this definition method is used to calculate the fatigue damage variable D of the jointed rock models. A schematic of the determination of the fatigue damage variable is shown in Fig. 5b, and the equation can be expressed as follows:

$$D = \frac{\sum_{i=1}^{N_i} |U_i^d|}{\sum_{i=1}^N |U_i^d|} \quad (6)$$

where N and N_i are the cycle number at final and current time step, respectively, and U_i^d is the hysteresis energy in the i th cycle.

3.2 Results of Static Monotonic Loading Tests

Monotonic loading tests are performed on four jointed rock specimens to obtain the static uniaxial compressive strength, which provides the reference values for subsequent cyclic loading parameters. The monotonic stress–strain curves of the tested jointed specimens are shown in Fig. 6, featuring a slowly increasing part up to the peak strength and then a dramatic decreasing post-failure

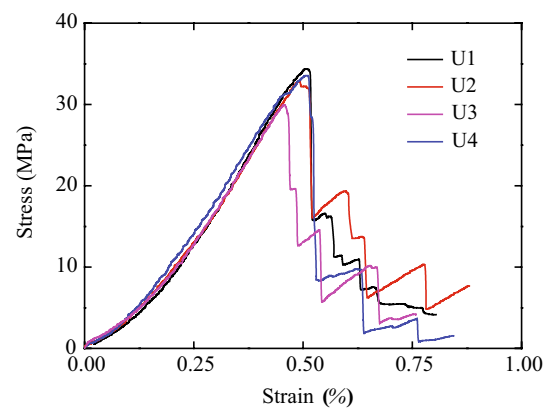


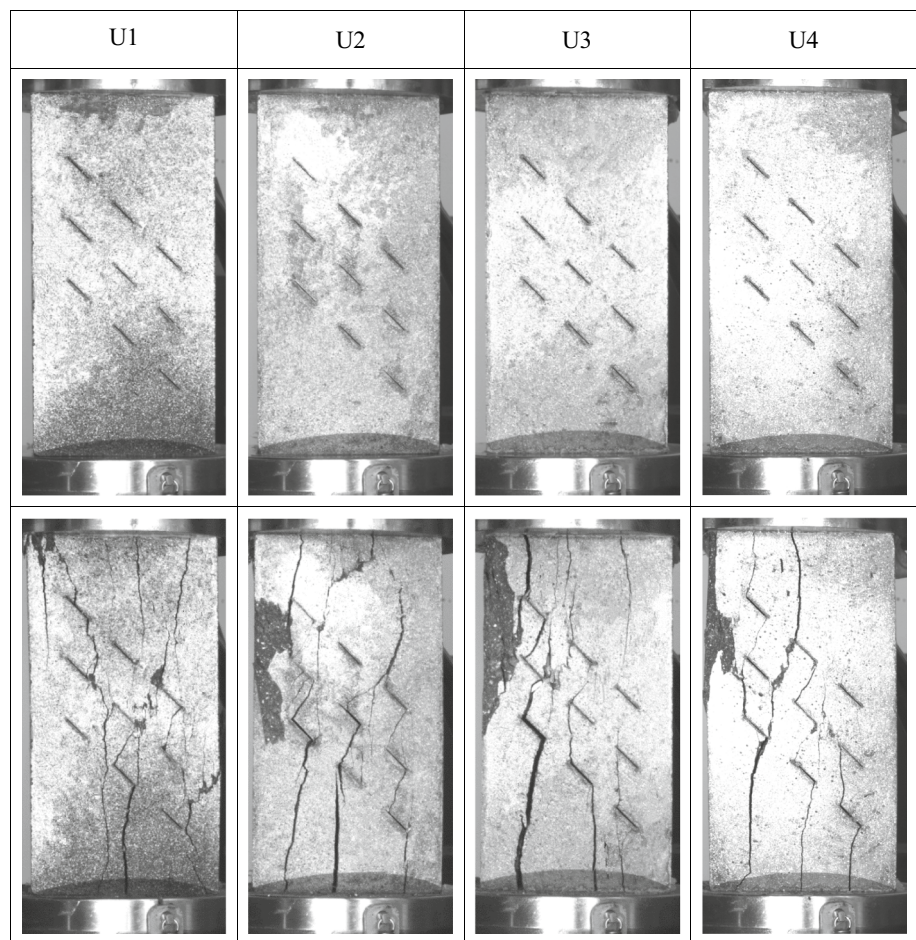
Fig. 6 Static uniaxial stress–strain curves of the four tested jointed rock specimens under monotonic loading

Table 2 Summary of monotonic uniaxial compression tests

Jointed specimen no.	Uniaxial compression strength (MPa)	Axial strain at failure point (%)	Young’s modulus (GPa)
U1	34.40	0.52	8.49
U2	33.05	0.52	7.74
U3	30.02	0.47	8.16
U4	33.59	0.50	8.13
Average	32.76	0.50	8.13

part. The details of experimental results are tabulated in Table 2, in which the measured average static uniaxial compressive strength is 32.76 MPa, and the average Young’s modulus is 8.13 GPa. Figure 7 depicts the failure

Fig. 7 Static uniaxial failure modes of the four tested jointed rock specimens under monotonic loading



modes at the peak strength of the four tested specimens under monotonic loading, in which the tensile splitting failure through intact materials is prominent in all tested specimens. Moreover, the four jointed specimens exhibit similar progressive failure behavior. Taking the specimen U4 as an example, Fig. 8 presents the progressive failure at six typical stress levels: i.e., initial state (i.e., 0 MPa), 20% peak strength (i.e., 6.72 MPa), 40% peak strength (i.e., 13.44 MPa), 60% peak strength (i.e., 20.15 MPa), 80% peak strength (i.e., 26.87 MPa), and 100% peak strength (i.e., 33.59 MPa). As the axial stress increases almost linearly up to 40% peak strength, the front surface of the tested specimen barely changes (Fig. 8a–c). At the stress level of 60% peak strength, the surface cracks initiate from the joint tips (Fig. 8d). Afterward, the axial stress continues to increase up to 80% peak strength, corresponding to the further propagation of cracks and the formation of the observable tensile wing cracks on the front surface of the tested specimen (Fig. 8e). As the stress reaches its maximum value, i.e., 100% peak strength, the wing cracks completely coalesce, triggering the inevitable tensile failure through the entire specimen (Fig. 8f).

4 Experimental Results and Discussion of Cyclic Uniaxial Compression Tests

To investigate the influence of cyclic loading parameters (i.e., loading frequency, maximum stress and amplitude) on the fatigue mechanical properties of intermittently jointed rock models, 10 different cyclic loading conditions are applied on the synthetic jointed rock models with the same geometrical parameters (i.e., $a = 15$ mm, $b = 20$ mm, $d = 24$ mm, $\theta = 45^\circ$, $k = 0.318$ and $\rho = 3$ rows). For each loading condition, three jointed rock models are tested. The specifics of cyclic uniaxial compression tests are listed in Table 1, and the corresponding results are reported and discussed in this section.

4.1 Influence of Cyclic Loads on the Fatigue Deformation Characteristics

Figure 9a–c shows the representative stress–strain curves of intermittently jointed specimens under monotonic loading and different cyclic loading conditions. During an entire cyclic test, the number of hysteresis loops in the fatigue

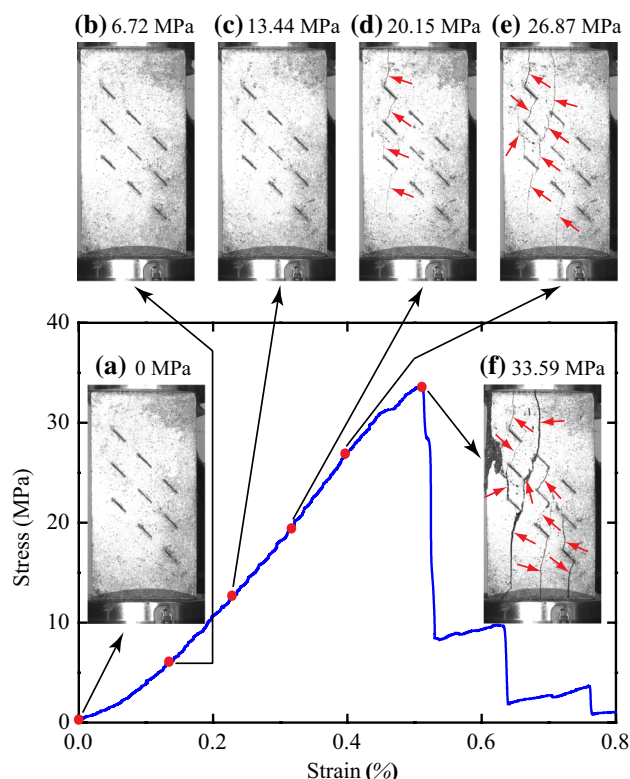


Fig. 8 Progressive failure behavior of the jointed rock specimen U4 under monotonic loading (red arrows indicate the surface cracks of the tested jointed specimen) (color figure online)

curve ranges from sparse to intensive and then to sparse. There are two parts of fatigue strain in each hysteresis loop, i.e., the elastic strain and the plastic strain; the elastic part is restored during the unloading progress, while the plastic part is irreversible and gradually accumulates with increasing cycles until the fatigue failure occurs. In addition, as shown in Fig. 10, the terminal fatigue strain (i.e., the axial strain at the fatigue failure point in the cyclic stress–strain curve) of the tested specimens is found to be approximately equal to the post-failure monotonic strain (i.e., the axial strain at the point with the maximum cyclic stress in the post-failure portion of the monotonic stress–strain curve). As compared in Table 1, the deviations between them are $<8\%$, which indicates that the fatigue deformations of the jointed rocks are dominated by their static deformations.

Similar to the three-phase development of irreversible deformations for intact rocks (Xiao et al. 2009), the irreversible plastic strains of the tested jointed rock specimens under different cyclic loading conditions also develop in a three-stage manner, i.e., initial, steady, and accelerated stage, as marked in Fig. 11. For a given loading condition, the irreversible strain increases rapidly in stage I and remains steady in stage II until it accelerates again in stage III due to the sudden fatigue failure. In the accelerated stage, the

irreversible strain increases more rapidly under cyclic loading conditions with higher maximum stress, higher amplitude, or lower cyclic frequency.

Figure 12 shows the influence of the three cyclic loading parameters on the two representative strains, i.e., initial and terminal irreversible strains; the two strains are defined as the irreversible strains accumulated in the initial stage and in all three stages, respectively. Specifically, as the loading frequency increases from 1 to 10 Hz, the initial and terminal irreversible strains increase from 0.27 to 0.34% and from 0.32 to 0.37%, respectively. In contrast, the two strains feature a linear decrease with increasing maximum cyclic stress; as the maximum stress level increases from 0.80 to 0.95, the initial and terminal irreversible strains decrease from 0.29 to 0.22% and from 0.35 to 0.27%, respectively. Similar to the influence of maximum stress, as the amplitude level increases from 0.40 to 0.70, the initial and terminal irreversible plastic strains decrease from 0.32 to 0.15% and from 0.36 to 0.18%, respectively.

Two representative fatigue deformation moduli of the jointed rock specimens are also analyzed, namely, Young's modulus and secant modulus. In this study, the Young's modulus is defined as the slope of straight-line portion of the stress–strain curve, and the secant modulus is the slope of secant line at a stress level at 50% of the static uniaxial compressive strength. Figure 13 presents the relationships between the two fatigue moduli and the relative cycle (i.e., ratio of the current cycle number n to the total cycle number N) of the jointed rock specimens under different cyclic loading conditions. All the curves of fatigue moduli show a nonlinear decrease with increasing relative cycle, and both the Young's modulus and the secant modulus decrease with increasing frequency or decreasing maximum stress and amplitude. In addition, compared with the variation of secant modulus, the Young's modulus is more susceptible to cyclic loading parameters.

4.2 Influence of Cyclic Loads on the Fatigue Energy Parameters

In this section, the fatigue energy parameters of jointed rock specimens under cyclic loading are determined employing Eq. (5), including the total energy density, the elastic energy density and the hysteresis energy density. Representative curves of energy density parameters of the tested jointed specimens under different cyclic loading conditions are depicted in Figs. 14 and 15, and the corresponding results are listed in Tables 3, 4, and 5. As shown in Fig. 14, as the relative cycle increases, the total energy density in a cycle decreases in the initial cycles, remains almost constant for a while, and then increases. In sharp contrast, the variation of the elastic energy density is opposite to that of the total energy density. Compared to that of the total energy density

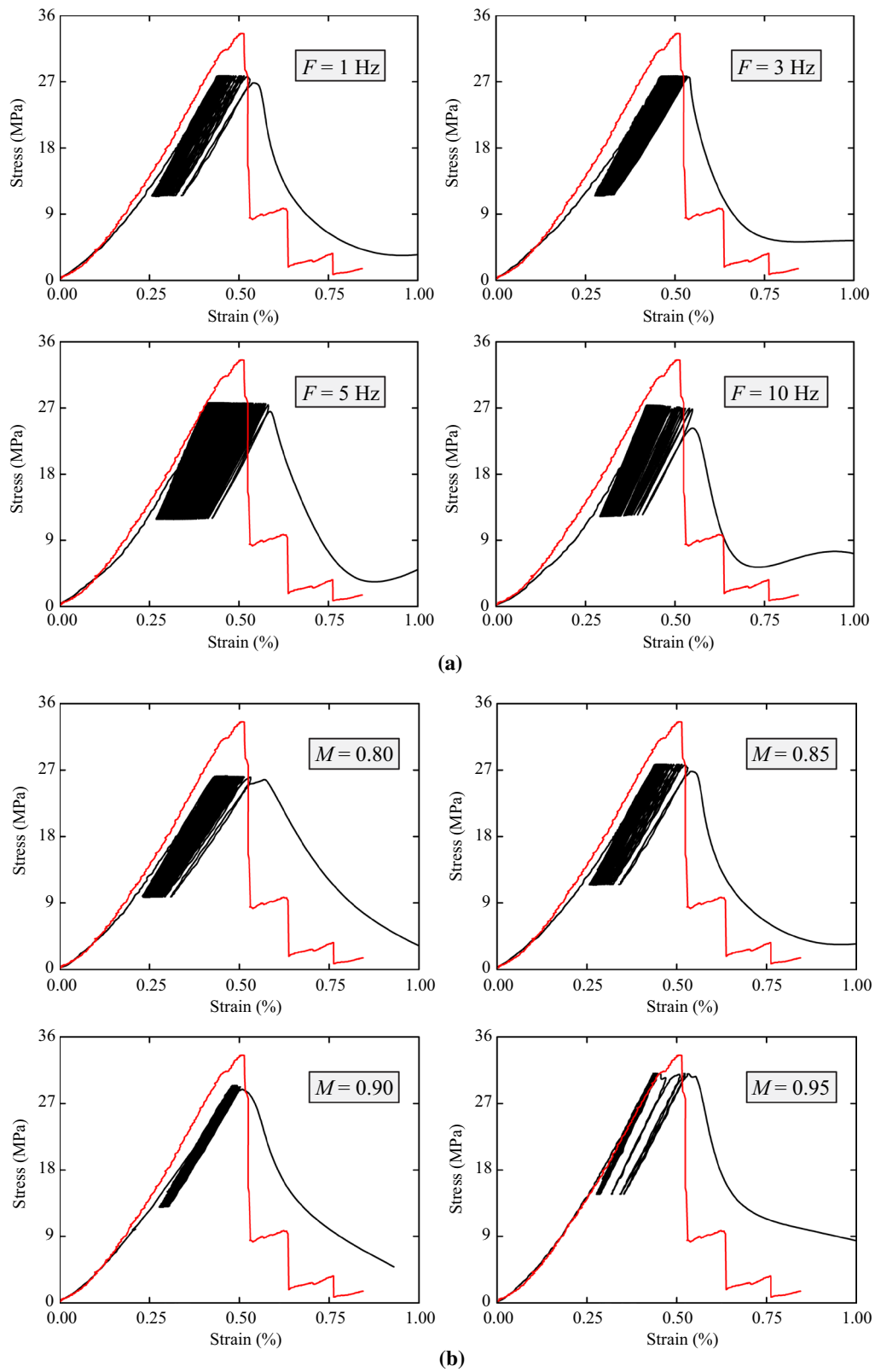


Fig. 9 Representative stress–strain curves of the jointed rock specimens obtained from monotonic and cyclic loading tests: **a** different loading frequencies, **b** different maximum stress levels, and **c** differ-

ent amplitude levels (red line and black line denote the monotonic stress–strain curve and the cyclic stress–strain curve, respectively) (color figure online)

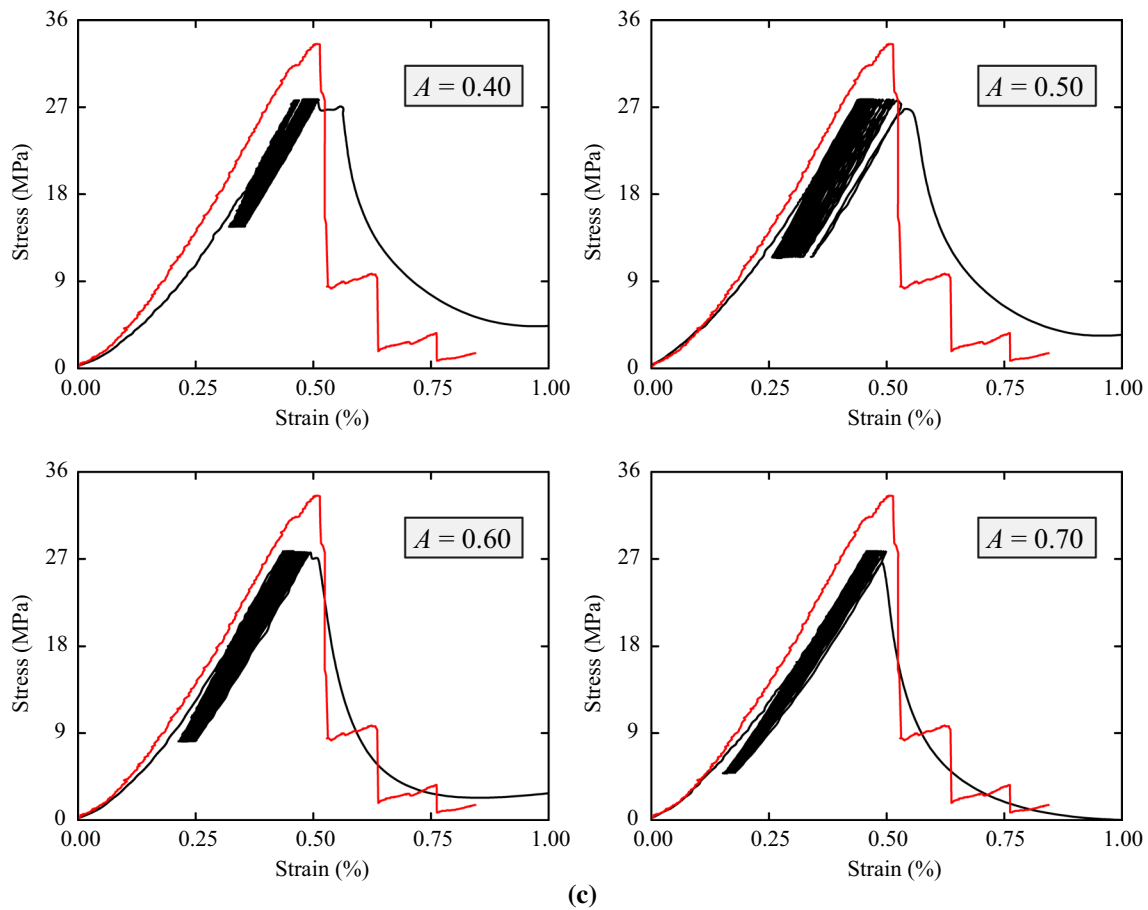


Fig. 9 (continued)

and the elastic energy density, the variation of the hysteresis energy density with respect to the relative cycle is more drastic. It features a dramatic increasing and decreasing transition in the initial cycles, and then it increases again (Fig. 15).

Moreover, the energy density magnitudes are highly dependent on cyclic loading parameters. As the loading frequency increases, the duration of cyclic loads acting on tested specimen becomes shorter, leading to the decrease in the total energy. Taking the fatigue energy density parameters in the initial stage to analyze, as the loading frequency increases from 1 to 10 Hz, the initial total energy density, elastic energy density, and hysteresis energy density decrease from 0.042 to 0.028 MJ/mm³, from 0.037 to 0.027 MJ/mm³, and from 0.005 to 0.001 MJ/mm³, respectively. In addition, as the maximum stress level increases from 0.80 to 0.95, the initial total energy density, elastic energy density, and hysteresis energy density increase from 0.037 to 0.059 MJ/mm³, from 0.034 to 0.043 MJ/mm³, and from 0.003 to 0.016 MJ/mm³, respectively. With increasing cyclic amplitude, more

energy is absorbed, and the area of hysteresis loop increases, indicating that more energy is released for fatigue failure of the tested specimen. Thus, as the amplitude level increases from 0.40 to 0.70, the initial total energy density, elastic energy density, and hysteresis energy density increase from 0.039 to 0.050 MJ/mm³, from 0.036 to 0.039 MJ/mm³, and from 0.003 to 0.011 MJ/mm³, respectively.

4.3 Influence of Cyclic Loads on the Fatigue Damage Evolution

Employing Eq. (6) in Sect. 3.2, the fatigue damage variables of jointed rock specimens can be calculated based on the hysteresis energy. Figure 16 depicts the corresponding cumulative damage evolution curves of the tested jointed specimens under different cyclic uniaxial compression; these curves show an inverted-S shape. Similar to the development of irreversible plastic strain of jointed rock specimens, these inverted-S-shaped curves can also be divided into three stages: initial, steady, and accelerated stages. The fatigue

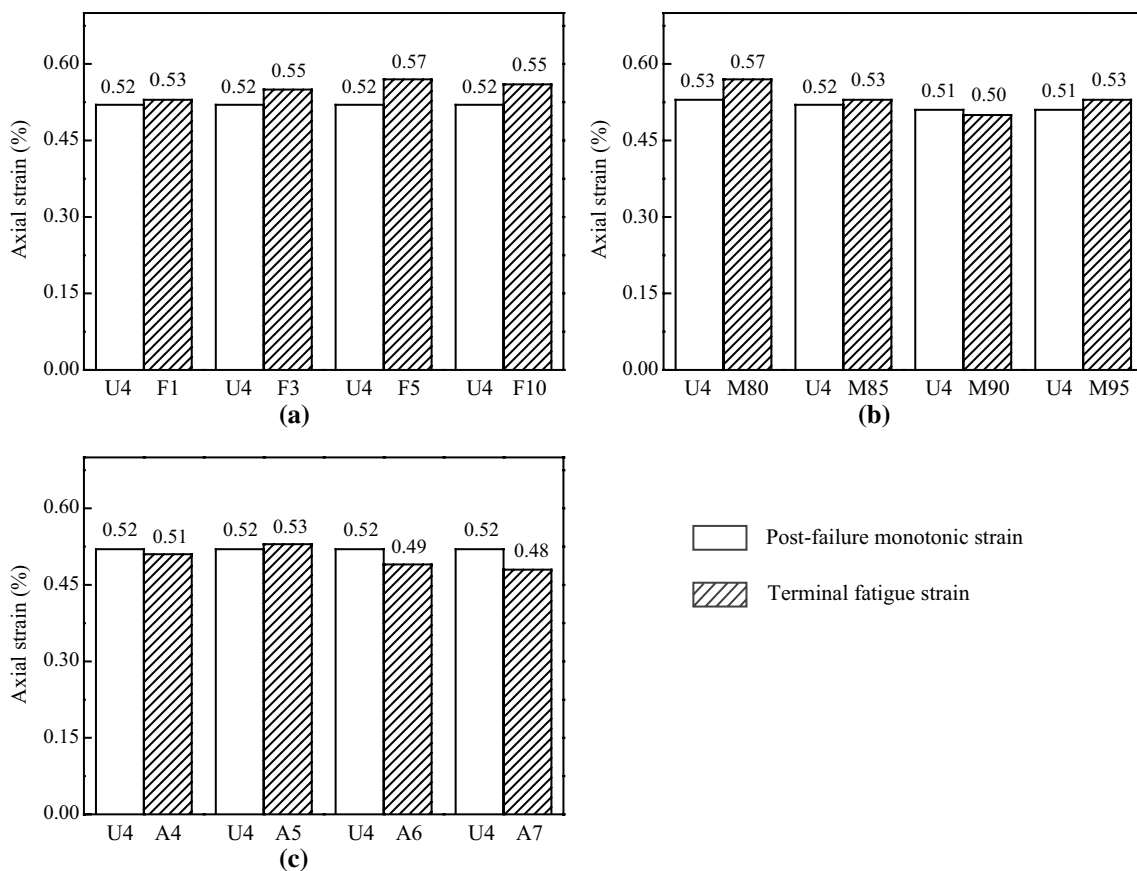


Fig. 10 Terminal fatigue strain of the tested jointed rock specimens under different cyclic loading conditions and the post-failure monotonic strain corresponding to maximum cyclic stress. Square, post-

failure monotonic strain. Square with bar, terminal fatigue strain. **a** Different loading frequencies. **b** Different maximum stress levels. **c** Different cyclic amplitude levels

damage variable accumulates quickly in the first stage, and then it increases steadily. In the third stage, the damage variable increases rapidly again as the final fatigue failure of the specimen occurs.

Considering the influence of the three cyclic loading parameters on the fatigue damage, Fig. 16 shows that the cumulative damage variable increases with decreasing frequency and increasing maximum stress or amplitude. The variation of fatigue damage with cyclic loading parameters can be explained as follows. Under a higher loading frequency, less energy is dissipated, leading to the decrease in damage variable. Specifically, as the loading frequency increases from 1 to 10 Hz, the damage variable in the initial stage decreases from 0.17 to 0.10. In sharp contrast, at a higher maximum stress or amplitude, more energy is released, resulting in the increase in the damage variable. Hence, as the maximum stress level and the amplitude level increase from 0.80 to 0.95 and from 0.40 to 0.70, respectively, the initial damage variable increases from 0.14 to 0.27 and from 0.13 to 0.21, respectively. Figure 16

also illustrates the relations between the fatigue lives (i.e., the number of cycles to fatigue failure) of jointed rock specimens and the three cyclic loading parameters. With increasing loading frequency or decreasing maximum stress and amplitude, the fatigue life of the tested jointed specimen shows an exponential increase; the specific values of fatigue lives under different cyclic loading parameters are listed in Table 1.

4.4 Influence of Cyclic Loads on the Fatigue Progressive Behavior

Figure 17a–c depicts the representative fatigue failure scenarios of jointed specimens under cyclic uniaxial compression with different loading parameters. In all cyclically failed jointed specimens, the tensile wing cracks are the primary cracks, similar to the tensile splitting failure of jointed specimens under monotonic loading (Fig. 7). These wing cracks propagate at a certain angle with the preexisting joints toward the direction of maximum compression (Sagong and

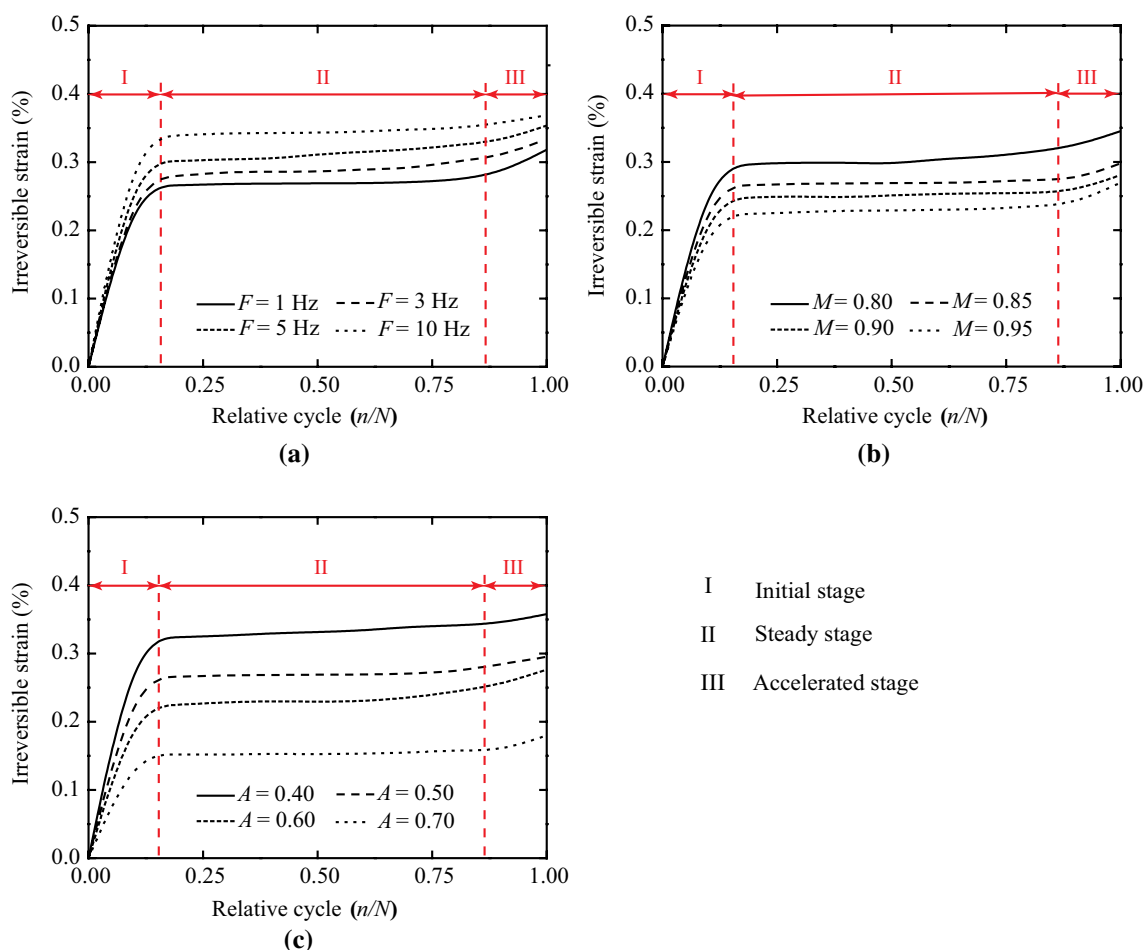


Fig. 11 Development curves of the irreversible plastic strains of jointed rock specimens under various cyclic loading conditions. *I* Initial stage. *II* Steady stage. *III* Accelerated stage. **a** Different loading frequencies. **b** Different maximum stress levels. **c** Different cyclic amplitude levels

Bobet 2002), leading to an inevitable tensile splitting failure through the intact materials. Based on the existing standard definition of crack coalescence categories proposed by Wong and Einstein (2009a), three different coalescence patterns are observed in this study. The classification schematics are shown in Fig. 18, and the representative coalescence patterns in our tests are depicted in Fig. 19. Category I denotes that the two preexisting joints are linked up by a T-I crack; this tensile wing crack probably initiates from the tip of joint 1 and then propagates toward the face of joint 2 at a distance from the joint tip (Fig. 18a), or it perhaps initiates from the face of joint 1 at a distance from the joint tip and then propagates toward the tip of joint 2 (Fig. 18b). In Category II, the joint tips are linked up at the same side by a T-II crack dominantly of tensile nature, forming almost a straight line along the axial loading direction (Fig. 18c); since this tensile crack occurs in the opposite direction to the conventional wing crack, it cannot be regarded as a T-I wing crack. In

contrast, for Category III, the joint tips are linked up at the opposite side, i.e., from the right tip of joint 1 to the left tip of joint 2 (Fig. 18d), forming an oblique T-III crack; the angle between the oblique T-III crack and the loading direction is larger than that between the straight T-II crack and the loading direction. Note that there may be occasional short shear cracks along the coalescence direction in Categories II and III.

Compared with the progressive failure behavior under the monotonic loading (Fig. 8), the fatigue failure of jointed specimens under cyclic loading usually occurs more abruptly without obvious preceding signs. Taking the jointed specimen F1 as an example, Fig. 20 depicts the progressive fatigue failure during six stages: i.e., initial stage, 20% fatigue life, 40% fatigue life, 60% fatigue life, 80% fatigue life, and 100% fatigue life. From stage I (initial stage) to stage III (40% fatigue life), no obvious variation can be observed on the front surface of tested

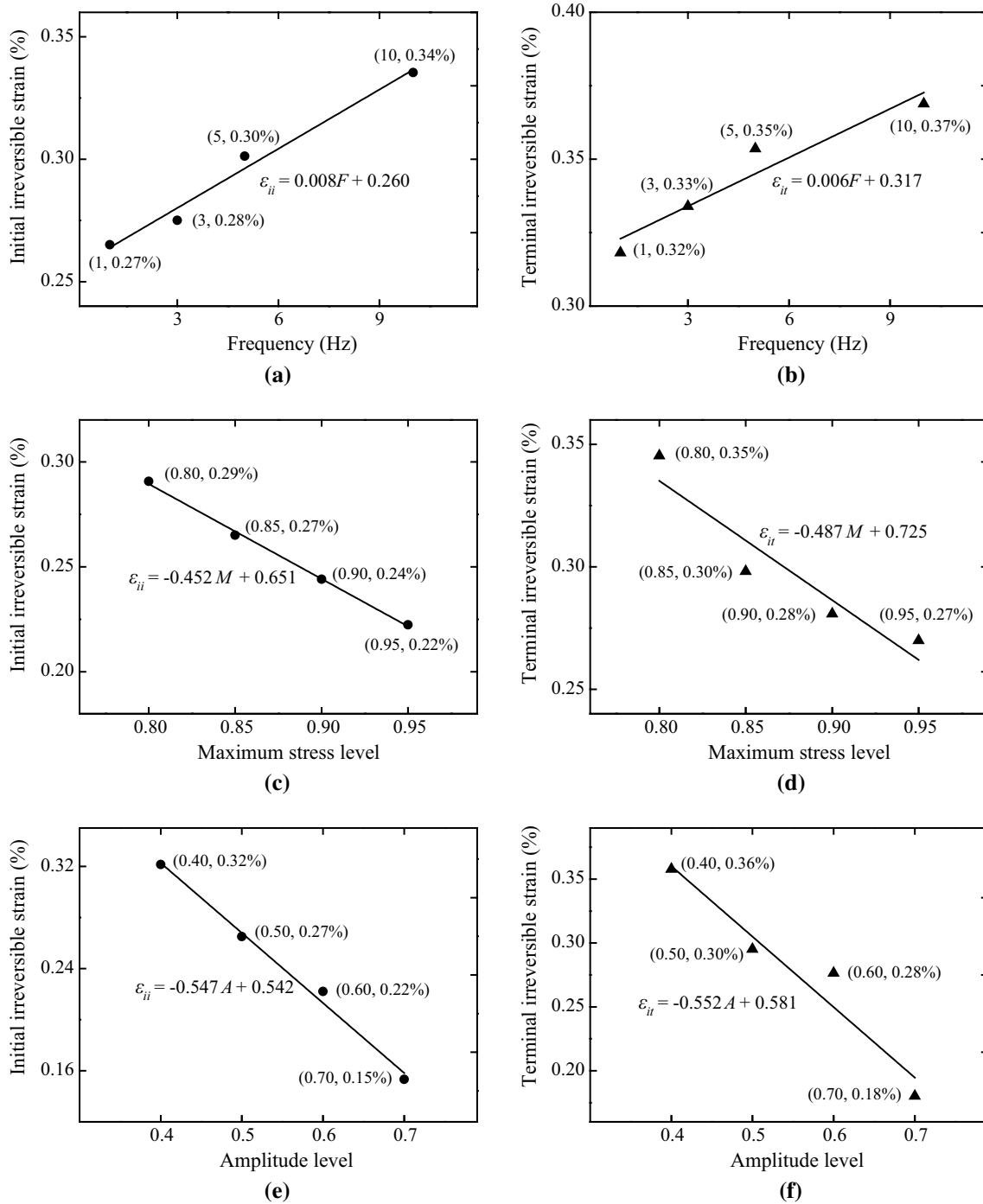


Fig. 12 Influence of cyclic loading parameters on the initial and terminal irreversible strains: **a, b** loading frequency, **c, d** maximum stress level, and **e, f** amplitude level

specimen, similar to the process that the axial stress increases from 0 to 40% peak strength in monotonic loading test (Fig. 8a–c). In stage IV (60% fatigue life), the surface cracks initiate from the joint tips due to the highly

concentrated stress, while these initiation cracks are less obvious than those under monotonic loading (Fig. 8d); after that, these cracks further propagate forming the observable tensile wing cracks through stage IV to stage

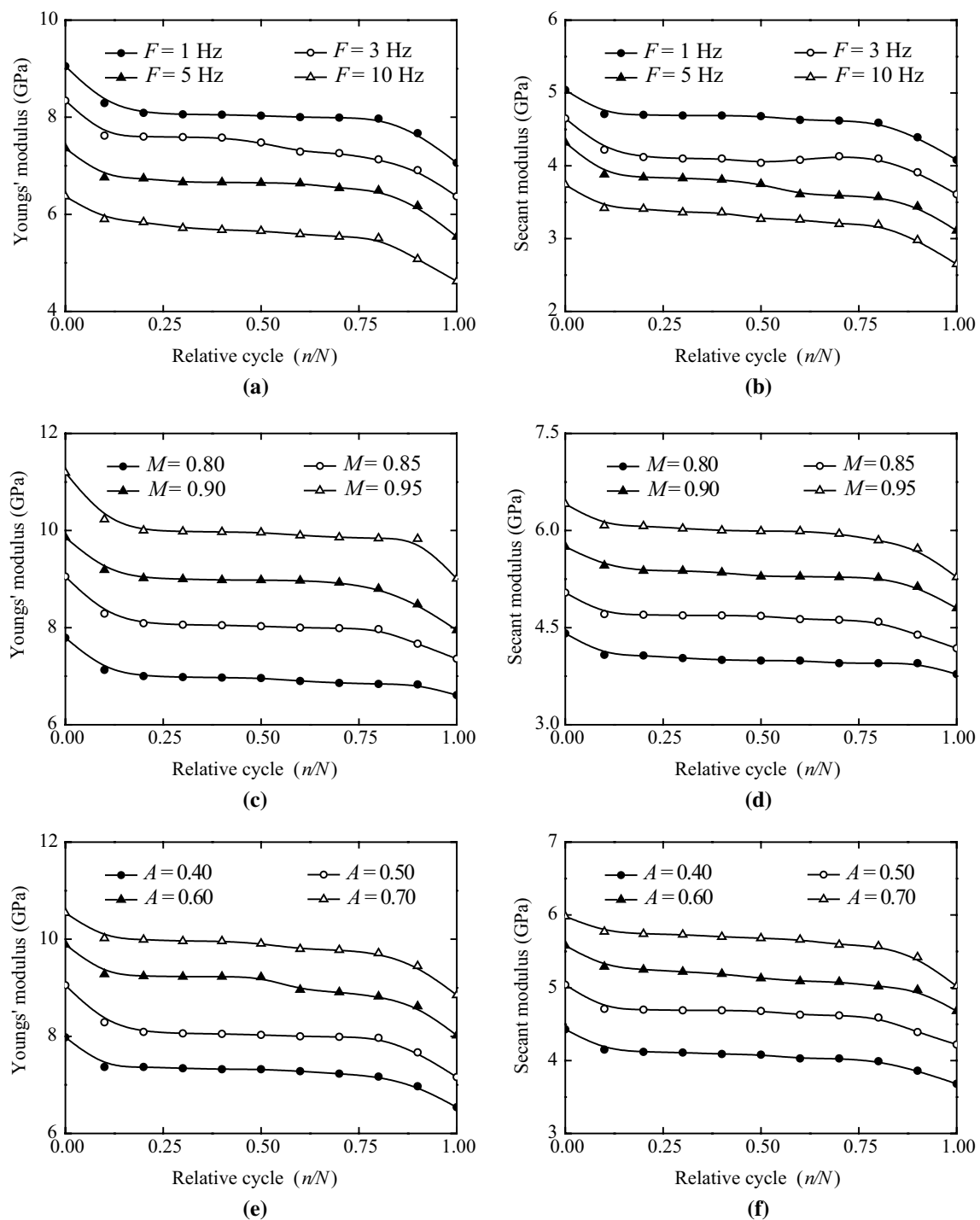


Fig. 13 Influence of cyclic loading parameters on the Young's modulus and secant modulus: **a** different loading frequencies, **b** different maximum stress levels, and **c** different amplitude levels

V (80% fatigue life). Rather than the gradual coalescence of surface cracks in monotonic loading tests, these surface tensile cracks of cyclically tested jointed specimens

close and open at the same pace as the loading frequency, eventually triggering the sudden fatigue failure at stage VI (100% fatigue life).

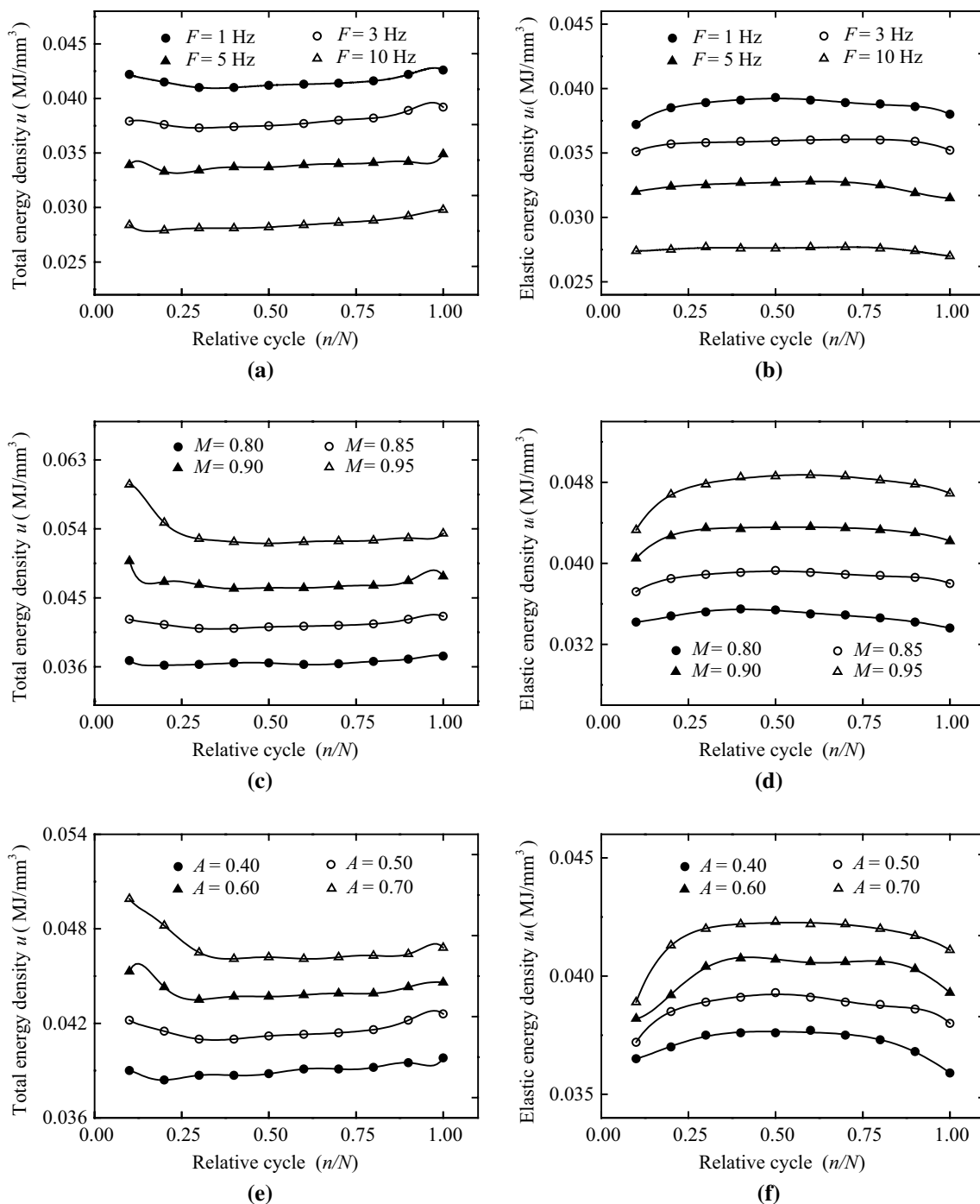


Fig. 14 Influence of cyclic loading parameters on the total energy density and the elastic energy density: **a, b** different loading frequencies, **c, d** different maximum stress levels, and **e, f** different amplitude levels

5 Summary and Conclusions

Intermittently jointed rocks are quite sensitive to cyclic loading conditions in mining and civil engineering structures. However, the systematic investigations on the fatigue mechanism of jointed rocks under different cyclic loading

are rather limited. In this study, synthetic jointed rock models are employed to perform cyclic uniaxial compression tests with different loading parameters, including four frequencies, four maximum stresses and four amplitudes. Our experimental results systematically depict the influence of the three cyclic loading parameters on the fatigue

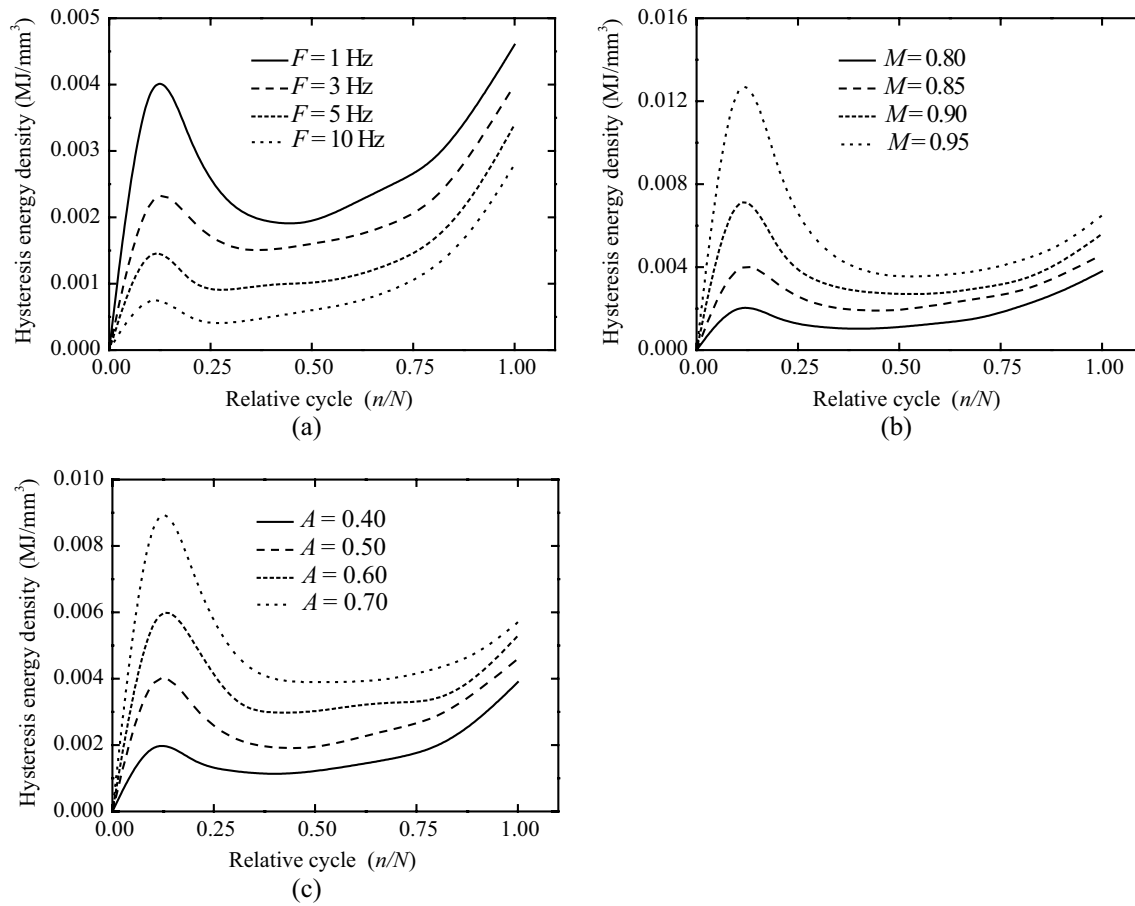


Fig. 15 Influence of cyclic loading parameters on the hysteresis energy density: **a** different loading frequencies, **b** different maximum stress levels, and **c** different amplitude levels

Table 3 Total energy density (MJ/mm^3) of the representative jointed rock specimens at different relative cycle

Jointed specimen no.	Relative cycle									
	0.1 N	0.2 N	0.3 N	0.4 N	0.5 N	0.6 N	0.7 N	0.8 N	0.9 N	1.0 N
F1 or M85 or A5	0.0422	0.0415	0.0410	0.0410	0.0412	0.0413	0.0414	0.0416	0.0422	0.0426
F3	0.0379	0.0376	0.0373	0.0374	0.0375	0.0377	0.0380	0.0382	0.0389	0.0392
F5	0.0339	0.0333	0.0334	0.0337	0.0337	0.0339	0.0340	0.0341	0.0342	0.0349
F10	0.0284	0.0279	0.0281	0.0281	0.0282	0.0284	0.0286	0.0288	0.0292	0.0298
M80	0.0368	0.0362	0.0363	0.0365	0.0365	0.0363	0.0364	0.0367	0.0370	0.0374
M90	0.0498	0.0471	0.0467	0.0462	0.0463	0.0463	0.0465	0.0466	0.0472	0.0478
M95	0.0598	0.0548	0.0527	0.0523	0.0521	0.0523	0.0524	0.0525	0.0528	0.0534
A4	0.0390	0.0384	0.0387	0.0387	0.0388	0.0391	0.0391	0.0392	0.0395	0.0398
A6	0.0453	0.0443	0.0435	0.0437	0.0437	0.0438	0.0439	0.0439	0.0443	0.0446
A7	0.0499	0.0482	0.0465	0.0461	0.0462	0.0461	0.0462	0.0463	0.0464	0.0468

Table 4 Elastic energy density (MJ/mm³) of the representative jointed rock specimens at different relative cycle

Jointed specimen no.	Relative cycle									
	0.1 N	0.2 N	0.3 N	0.4 N	0.5 N	0.6 N	0.7 N	0.8 N	0.9 N	1.0 N
F1 or M85 or A5	0.0372	0.0385	0.0389	0.0391	0.0393	0.0391	0.0389	0.0388	0.0386	0.0380
F3	0.0351	0.0357	0.0358	0.0359	0.0359	0.0360	0.0361	0.0360	0.0359	0.0352
F5	0.0320	0.0324	0.0325	0.0327	0.0327	0.0328	0.0327	0.0325	0.0319	0.0315
F10	0.0274	0.0275	0.0277	0.0276	0.0276	0.0277	0.0277	0.0276	0.0274	0.0270
M80	0.0342	0.0348	0.0352	0.0355	0.0354	0.0350	0.0349	0.0346	0.0342	0.0336
M90	0.0405	0.0427	0.0435	0.0434	0.0436	0.0436	0.0435	0.0433	0.0430	0.0422
M95	0.0433	0.468	0.0478	0.0485	0.0486	0.0487	0.0486	0.0482	0.0478	0.0469
A4	0.0365	0.0370	0.0375	0.0376	0.0376	0.0377	0.0375	0.0373	0.0368	0.0359
A6	0.0382	0.0392	0.0404	0.0408	0.0407	0.0406	0.0406	0.0406	0.0403	0.0393
A7	0.0389	0.0413	0.0420	0.0422	0.0423	0.0422	0.0422	0.0420	0.0417	0.0411

Table 5 Hysteresis energy density (MJ/mm³) of the representative jointed rock specimens at different relative cycle

Jointed specimen no.	Relative cycle									
	0.1 N	0.2 N	0.3 N	0.4 N	0.5 N	0.6 N	0.7 N	0.8 N	0.9 N	1.0 N
F1 or M85 or A5	0.0050	0.0030	0.0021	0.0019	0.0019	0.0022	0.0025	0.0027	0.0036	0.0046
F3	0.0028	0.0019	0.0015	0.0015	0.0016	0.0017	0.0019	0.0022	0.0030	0.0040
F5	0.0019	0.0009	0.0009	0.0010	0.0010	0.0011	0.0013	0.0016	0.0023	0.0034
F10	0.0010	0.0004	0.0004	0.0005	0.0006	0.0007	0.0009	0.0012	0.0018	0.0028
M80	0.0026	0.0014	0.0011	0.0010	0.0011	0.0013	0.0015	0.0021	0.0028	0.0038
M90	0.0093	0.0044	0.0032	0.0028	0.0027	0.0027	0.0030	0.0033	0.0042	0.0056
M95	0.0165	0.0080	0.0049	0.0038	0.0035	0.0036	0.0038	0.0043	0.0050	0.0065
A4	0.0025	0.0014	0.0012	0.0011	0.0012	0.0014	0.0016	0.0019	0.0027	0.0039
A6	0.0071	0.0051	0.0031	0.0029	0.0030	0.0032	0.0033	0.0033	0.0040	0.0053
A7	0.0110	0.0069	0.0045	0.0039	0.0039	0.0039	0.0040	0.0043	0.0047	0.0057

properties of intermittently jointed rock models, regarding the fatigue deformation characteristic, the fatigue energy and damage evolution, and the fatigue failure and progressive behavior. The following conclusions can be drawn:

1. The terminal fatigue strain (i.e., the axial strain at the fatigue failure point in the cyclic stress–strain curve) of the tested specimens is approximately equal to the post-failure monotonic strain (i.e., the axial strain at the point with the maximum cyclic stress in the post-failure portion of the monotonic stress–strain curve). Both the Young’s modulus and the secant modulus feature a non-linear decrease with increasing cycles, and the development of irreversible plastic strain can be divided into three stages, i.e., initial, steady, and accelerated stages (Figs. 9, 10, 11, 12, 13, 14).
2. The total energy density in each cycle decreases in the initial cycles, remains almost constant for a while, and then increases, while the variation of the elastic energy density is the opposite. The hysteresis energy density features a dramatic increasing and decreasing transition and then increases again. The three energy density parameters increase as the frequency decreases or the maximum cyclic stress and amplitude increase (Fig. 15).
3. Cumulative fatigue damage of jointed rock models exhibits an inverted-S shape with a three-stage evolution. This damage variable increases quickly in the initial cycles and then increases slowly until it increases

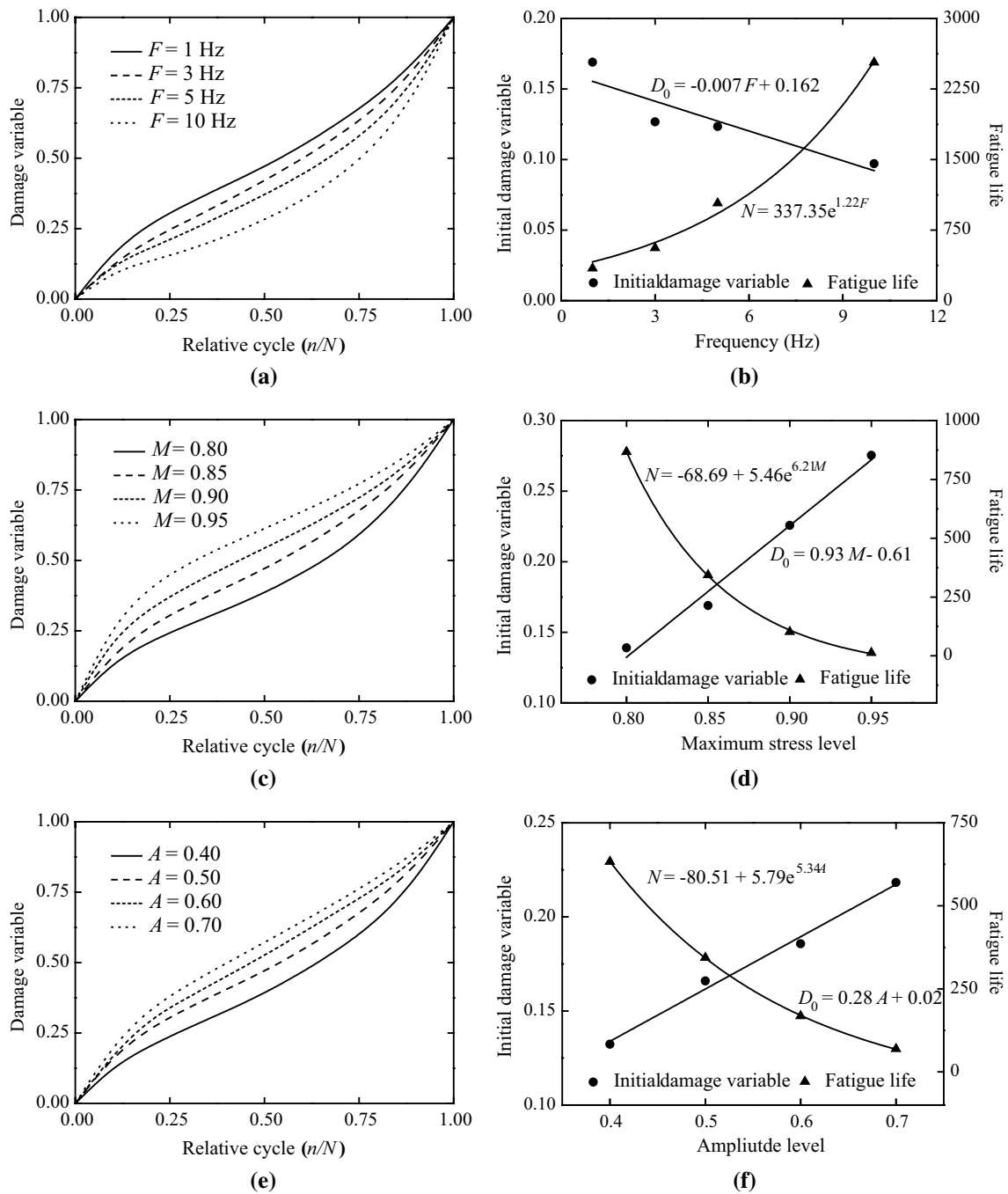
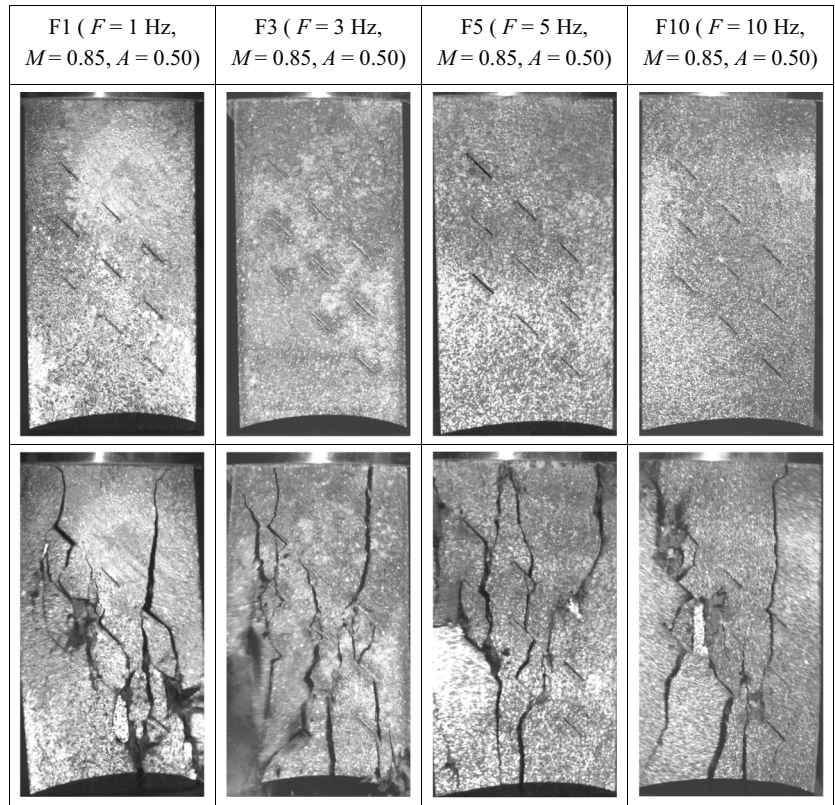


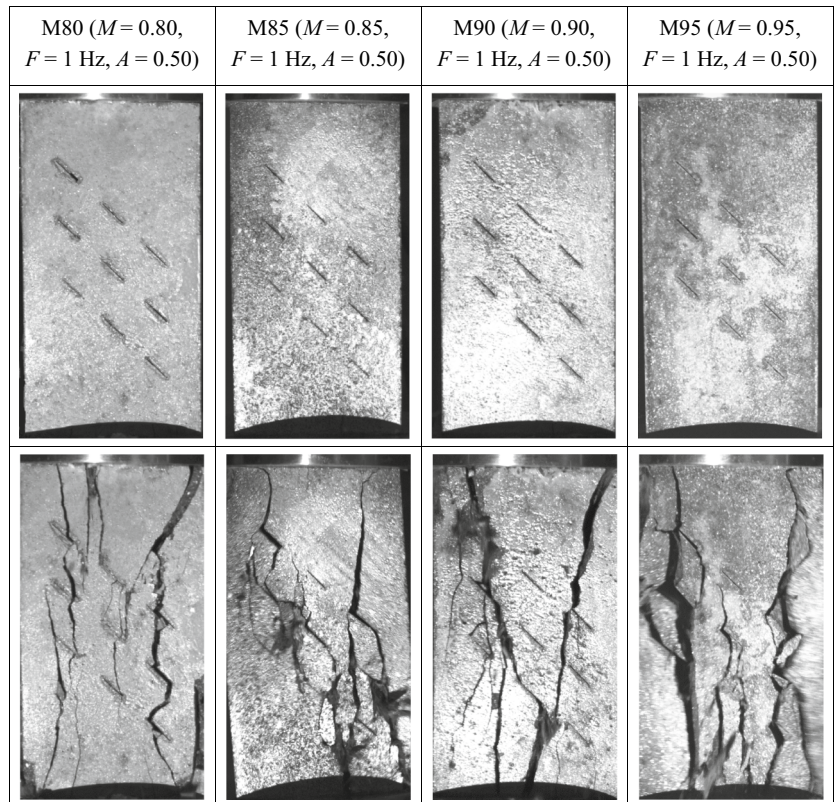
Fig. 16 Evolution of the fatigue damage variable of the jointed rock specimen under various cyclic loading conditions, and the influence of cyclic loading parameters on the initial damage variable and

fatigue life: **a, b** different loading frequencies, **c, d** different maximum stress levels, and **e, f** different amplitude levels

Fig. 17 Representative fatigue failure modes of the jointed rock specimens under various cyclic compression tests: **a** different loading frequencies, **b** different maximum stress levels, and **c** different amplitude levels



(a)



(b)

Fig. 17 (continued)

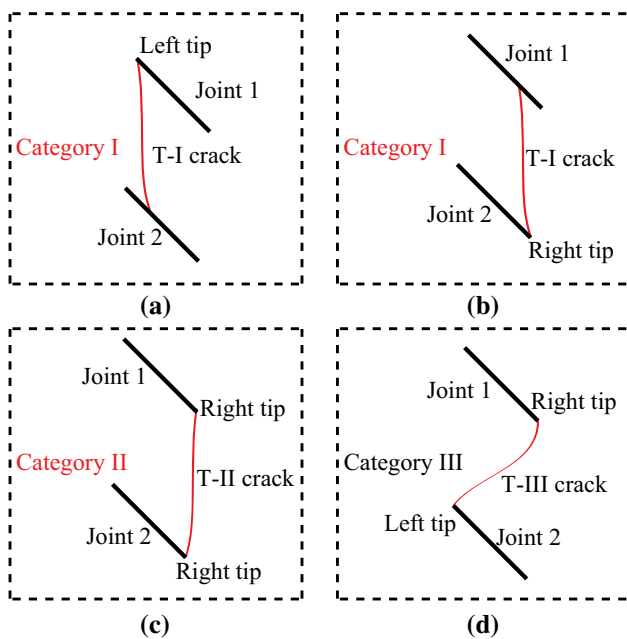
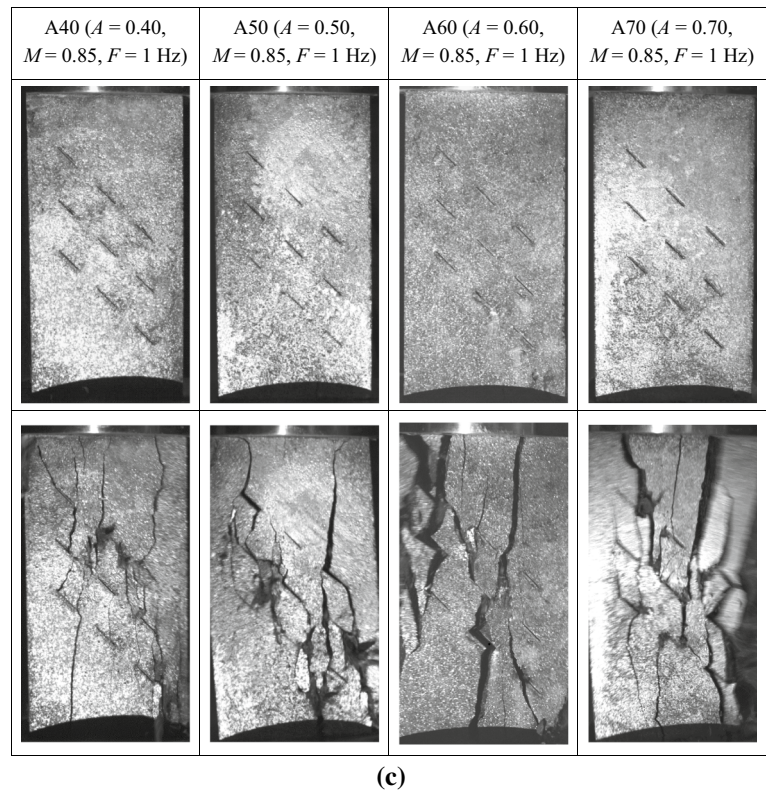


Fig. 18 Characteristic graphs of the crack coalescence categories observed in the present study: **a, b** Category I, **c** Category II, and **d** Category III

rapidly again as the fatigue failure of the specimen occurs. With decreasing frequency or increasing maximum stress and amplitude, the cumulative fatigue damage variable increases, leading to the decrease in fatigue life (Fig. 16).

4. Tensile splitting failure through intact materials is prominent in all cyclically failed jointed models, and three crack coalescence patterns are observed based on the interaction between two adjacent joints. The tensile cracks on the front surface of jointed specimens always initiate from joint tips and then propagate at a certain angle with the joints toward the direction of maximum compression (Figs. 17, 18, 19, 20).

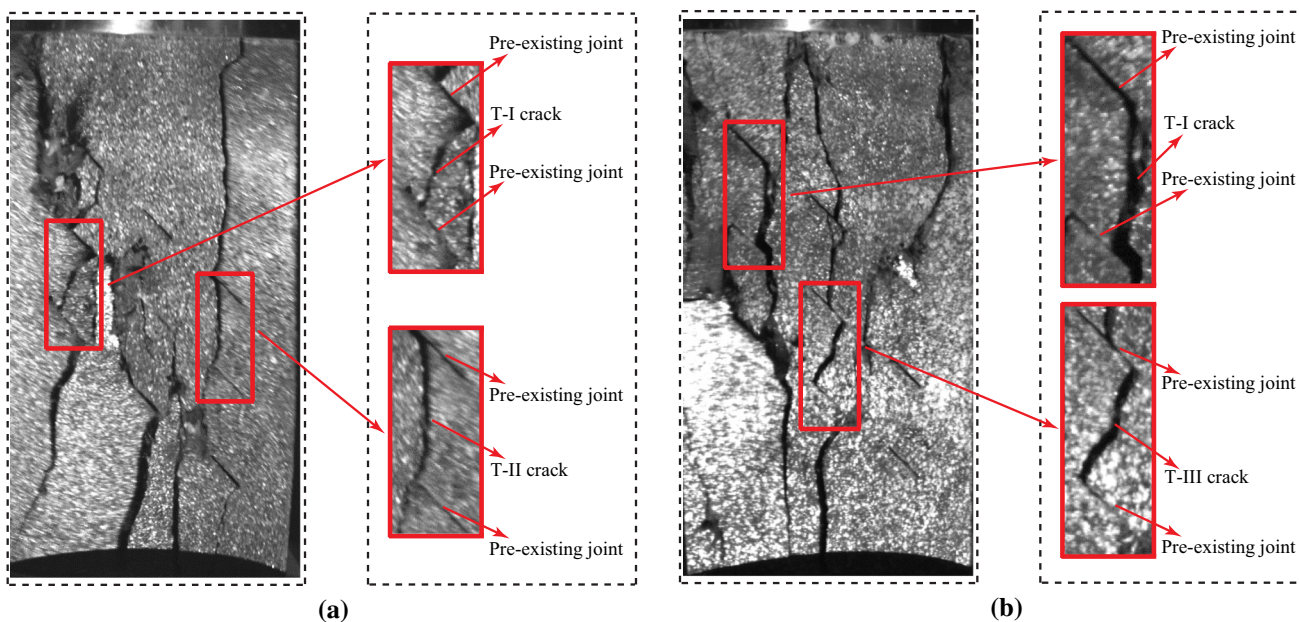


Fig. 19 Representative crack coalescence patterns observed in the present study

Initial stage	20% Fatigue life	40% Fatigue life
60% Fatigue life	80% Fatigue life	100% Fatigue life

Fig. 20 Progressive failure behavior of the jointed rock specimen F1 under cyclic uniaxial compression (red arrows indicate the surface cracks of the tested jointed specimen) (color figure online)

Acknowledgements The authors are grateful for the financial support from the National Program on Key Basic Research Project (No. 2015CB057903) and National Natural Science Foundation of China (No. 51779164 and No. 51374149).

References

Attewell PB, Farmer IW (1973) Fatigue behaviour of rock. *Int J Rock Mech Min Sci* 10:1–9

Bagde MN, Petroš V (2005a) Fatigue properties of intact sandstone samples subjected to dynamic uniaxial cyclical loading. *Int J Rock Mech Min Sci* 42(2):237–250

Bagde MN, Petroš V (2005b) Waveform effect on fatigue properties of intact sandstone in uniaxial cyclical loading. *Rock Mech Rock Eng* 38(3):169–196

Bagde MN, Petroš V (2009) Fatigue and dynamic energy behaviour of rock subjected to cyclical loading. *Int J Rock Mech Min Sci* 46(1):200–209

Bahaaddini M, Sharrock G, Hebblewhite BK (2013) Numerical investigation of the effect of joint geometrical parameters on the mechanical properties of a non-persistent jointed rock mass under uniaxial compression. *Comput Geotech* 49:206–225

Bahaaddinia M, Hagana PC, Mitraa R, Hebblewhite BK (2014) Scale effect on the shear behaviour of rock joints based on a numerical study. *Eng Geol* 181:212–223

Bi J, Zhou XP, Qian QH (2016) The 3D numerical simulation for the propagation process of multiple pre-existing flaws in rock-like materials subjected to biaxial compressive loads. *Rock Mech Rock Eng* 49(5):1611–1627

Bobet A, Einstein HH (1998) Fracture coalescence in rock-type material under uniaxial and biaxial compression. *Int J Rock Mech Min Sci* 35(7):863–888

Brown ET, Hudson JA (1974) Fatigue failure characteristics of some models of jointed rock. *Earthq Eng Struct Dyn* 2:379–386

Burdine NT (1963) Rock failure under dynamic loading conditions. *Soc Pet Eng J* 3:1–8

- Cao RH, Cao P, Lin H, Pu CZ, Ou K (2016) Mechanical behavior of brittle rock-like specimens with pre-existing fissures under uniaxial loading: experimental studies and particle mechanics approach. *Rock Mech Rock Eng* 49:763–783
- Dershowitz WS, Einstein HH (1988) Characterizing rock joint geometry with joint system models. *Rock Mech Rock Eng* 21(1):21–51
- Einstein HH, Hirschfeld RC (1973) Model studies on mechanics of jointed rock. *J Soil Mech Found Div ASCE* 99:229–248
- Einstein HH, Nelson RA, Bruhn RW, Hirschfeld RC (1969) Model studies of jointed rock behavior. In: *Proceedings of 11th symposium on rock mechanics*, pp 83–103
- Fan X, Kulatilake PHSW, Chen X (2015) Mechanical behavior of rock-like jointed blocks with multi-non-persistent joints under uniaxial loading: a particle mechanics approach. *Eng Geol* 190:17–32
- Feng P, Dai F, Liu Y, Xu NW, Fan PX (2017) Effects of coupled static and dynamic strain rates on the mechanical behaviors of rock-like specimens containing preexisting fissures under uniaxial compression. *Can Geotechn J*. doi:10.1139/cgj-2017-0286
- Fuenkajorn K, Phueakphum D (2010) Effects of cyclic loading on mechanical properties of Maha Sarakham salt. *Eng Geol* 112:43–52
- Gehle C, Kutter HK (2003) Breakage and shear behaviour of intermittent rock joints. *Int J Rock Mech Min Sci* 40:687–700
- Hua AZ, You MQ (2001) Rock failure due to energy release during unloading and application to underground rock burst control. *Tunn Undergr Space Technol* 16:241–246
- Kulatilake PHSW, He W, Um J, Wang H (1997) A physical model study of jointed rock mass strength under uniaxial compressive loading. *Int J Rock Mech Min Sci* 34(3):165.e1–165.e15
- Kulatilake PHSW, Malama B, Wang JL (2001) Physical and particle flow modeling of jointed rock block behavior under uniaxial loading. *Int J Rock Mech Min Sci* 38:641–657
- Lajtai EZ (1969) Strength of discontinuous rocks in direct shear. *Geotechnique* 19(2):218–233
- Li N, Chen W, Zhang P, Swoboda G (2001) The mechanical properties and a fatigue-damage model for jointed rock masses subjected to dynamic cyclical loading. *Int J Rock Mech Min Sci* 38:1071–1079
- Liu Y, Dai F, Zhao T, Xu NW (2017a) Numerical investigation of the fatigue properties of intermittent jointed rock models subjected to cyclic uniaxial compression. *Rock Mech Rock Eng* 50:89–112
- Liu Y, Dai F, Fan PX, Xu NW, Dong L (2017b) Experimental investigation of the influence of joint geometric configurations on the mechanical properties of intermittent jointed rock models under cyclic uniaxial compression. *Rock Mech Rock Eng* 50:1453–1471
- Ma JL, Liu XY, Wang MY, Xu HF, Hua RP, Fan PX, Jiang SR, Wang GA, Yi QK (2013) Experimental investigation of the mechanical properties of rock salt under triaxial cyclic loading. *Int J Rock Mech Min Sci* 62:34–41
- Meng QB, Zhang MW, Han LJ, Pu H, Nie TY (2016) Effects of acoustic emission and energy evolution of rock specimens under the uniaxial cyclic loading and unloading compression. *Rock Mech Rock Eng* 49(10):3873–3886
- Momeni A, Karakus M, Khanlari GR, Heidari M (2015) Effects of cyclic loading on the mechanical properties of a granite. *Int J Rock Mech Min Sci* 77:89–96
- Park JW, Song JJ (2009) Numerical simulation of a direct shear test on a rock joint using a bonded-particle model. *Int J Rock Mech Min Sci* 46:1315–1328
- Prost CL (1988) Jointing at rock contacts in cyclic loading. *Int J Rock Mech Min Sci Geomech Abstr* 25(5):263–272
- Prudencio M, Van Sint Jan M (2007) Strength and failure modes of rock mass models with non-persistent joints. *Int J Rock Mech Min Sci* 44:890–902
- Ray SK, Sarkar M, Singh TN (1999) Effect of cyclic loading and strain rate on the mechanical behaviour of sandstone. *Int J Rock Mech Min Sci* 36(4):543–549
- Sagong M, Bobet A (2002) Coalescence of multiple flaws in a rock-model material in uniaxial compression. *Int J Rock Mech Min Sci* 39:229–241
- Sagong M, Park D, Yoo J, Lee JS (2011) Experimental and numerical analyses of an opening in a jointed rock mass under biaxial compression. *Int J Rock Mech Min Sci* 48:1055–1067
- Shen B, Stephansson O, Einstein HH, Ghahreman B (1995) Coalescence of fractures under shear stresses in experiments. *J Geophys Res* 100(B4):5975–5990
- Singh M, Rao KS, Ramamurthy T (2002) Strength and deformational behaviour of a jointed rock mass. *Rock Mech Rock Eng* 35(1):45–64
- Singha M, Rao KS (2005) Empirical methods to estimate the strength of jointed rock masses. *Eng Geol* 77:127–137
- Solecki R, Conant RJ (2003) *Advanced mechanics of materials*. Oxford University Press, London
- Tao ZY, Mo HH (1990) An experimental study and analysis of the behaviour of rock under cyclic loading. *Int J Rock Mech Min Sci Geomech Abstr* 27(1):51–56
- Tiwari RP, Rao KS (2006) Post failure behaviour of a rock mass under the influence of triaxial and true triaxial confinement. *Eng Geol* 84:112–129
- Wong RHC, Chau KT (1998) Crack coalescence in a rock-like material containing two cracks. *Int J Rock Mech Min Sci* 35(2):147–164
- Wong LNY, Einstein HH (2009a) Crack coalescence in molded gypsum and Carrara marble: part 1. Macroscopic observations and interpretation. *Rock Mech Rock Eng* 42(3):475–511
- Wong LNY, Einstein HH (2009b) Crack coalescence in molded gypsum and Carrara marble: part 2. Microscopic observations and interpretation. *Rock Mech Rock Eng* 42(3):513–545
- Wong LNY, Einstein HH (2009c) Systematic evaluation of cracking behavior in specimens containing single flaws under uniaxial compression. *Int J Rock Mech Min Sci* 46:239–249
- Wong RHC, Chau KT, Tang CA, Lin P (2001) Analysis of crack coalescence in rock-like materials containing three flaws—part I: experimental approach. *Int J Rock Mech Min Sci* 38:909–924
- Wong RHC, Jiao MR, Chau KT (2006) Numerical and experimental study on progressive failure of marble. *Pure Appl Geophys* 163:1787–1801
- Xiao JQ, Ding DX, Xu G, Jiang FL (2009) Inverted S-shaped model for nonlinear fatigue damage of rock. *Int J Rock Mech Min Sci* 46(3):643–648
- Xiao JQ, Ding DX, Jiang FL, Xu G (2010) Fatigue damage variable and evolution of rock subjected to cyclic loading. *Int J Rock Mech Min Sci* 47(3):461–468
- Zhang XP, Wong LNY (2012) Cracking processes in rock-like material containing a single flaw under uniaxial compression: a numerical study based on bonded-particle model approach. *Rock Mech Rock Eng* 45:711–737
- Zhang XP, Wong LNY (2013) Crack initiation, propagation and coalescence in rock-like material containing two flaws: a numerical study based on bonded-particle model approach. *Rock Mech Rock Eng* 46:1001–1021
- Zhang HQ, Zhao ZY, Tang CA, Song L (2006) Numerical study of shear behavior of intermittent rock joints with different geometrical parameters. *Int J Rock Mech Min Sci* 43:802–816